Spin-polarized tunneling into helical edge states: asymmetry and conductances

D.N. Aristov[1, 2] and R.A. Niyazov[1, 3]

[1] *NRC "Kurchatov Institute", Petersburg Nuclear Physics Institute, Gatchina 188300, Russia*
[2] *St.Petersburg State University, 7/9 Universitetskaya nab., St. Petersburg, 199034 Russia*
[3] *Landau Institute for Theoretical Physics, Russian Academy of Sciences, Chernogolovka, Moscow oblast, 142432 Russia*

(Dated: January 2, 2017)

We consider tunneling from the spin-polarized tip into the Luttinger liquid edge state of quantum spin Hall system. This problem was previously studied in context of the spin and charge fractionalization of injected electron. Employing the fermionic approach and scattering states formalism for the appearing Y-junction, we calculate the renormalization of the dc conductances of the system. Our analysis confirms previous results for the scaling dependence of conductances in the lowest order of tunneling amplitude. Going beyond the lowest order we show that interaction affects not only the total tunneling rate, but also the asymmetry of the injected current. The scaling laws for the tunneling rate and for the asymmetry are different and we find the implicit function connecting both quantities during the renormalization. The topological nature of the helical edge state forbids the backscattering, which leads to the possibility of two stable fixed points in renormalization group sense, in contrast to the Y-junction between usual quantum wires.

arXiv:1612.09594v1 [cond-mat.str-el] 30 Dec 2016

I. INTRODUCTION

Topological insulators (TI) is a class of materials apparently important for future electronic devices.[1,2] Being insulator in the bulk, the TI necessarily has conducting states on its edge. The spin-orbit interaction leads to electrons spin-momentum locking in the edge states creating so called helical states. Backscattering on the nonmagnetic impurities in the same channel of such edge states is absent due to TI time-reversal symmetry. It allows a creation of devices with a lossless electron transport.

Electrons on the edge of 2D TI are confined to one spatial dimension (1D). One dimensional electron transport near the Fermi energy is described by well-known Tomonoga-Luttinger liquid (TLL) model.[3] The TLL corresponds to strongly correlated electron matter, and the 1D helical edge states add new peculiarities to it. This explains large experimental and theoretical interest to helical TLLs, with several suggested ways of probing their strongly correlated nature. Investigating the helical edge states was theoretically proposed by means of magnetic field in[4–6], by specific spatial construction of helical state in[7–9] and by quantum dots in[10,11].

Another natural way of probing – tunneling from the tip into the edge state – attracted a lot of attention. There is experimental evidence[12] and theoretical explanation[13] that the electron injection even into usual TLL may be characterized by charge fractionalization resulting in the currents imbalance. For helical TLL probing by the tip was considered theoretically in papers[14–19]. Experimentally it was confirmed that TI edge state is a quantum spin Hall state[20] , helical behavior of the edge state was observed in[21], the STM experiments were reported in [22] .

The transport properties of TLL model may be studied in two main approaches. The bosonization approach[3] takes into account the electron interaction exactly, the impurities are regarded as perturbation. The fermionic approach treats interaction perturbatively and studies the renormalization of impurities/junctions in S matrix formalism of asymptotic electronic states. Transport in quantum point contact is described by the conductances (transparencies) of junctions. The problem with one impurity in quantum wire can also be interpreted as the point contact of two wires. The latter case was considered within TLL model in bosonization[23–25] and fermionic[26,27] approaches. The conclusion of both approaches is that repulsive interaction renormalizes bare conductance to zero (total reflection case) whereas the attractive interaction leads to perfect transmission in the low temperature limit.

Further studies of usual TLL in bosonization approach addressed Y-junction with equal interaction constant[28] and arbitrary interaction in three wires[29]. The corner junction of helical TLLs was considered for two TI's in [30–32].

In the fermionic approach the renormalization group (RG) equations for S matrix characterizing the junction for arbitrary number of quantum wires was presented in [33,34]. Conductances of Y and X junctions were analyzed in the first order of interaction.

Partial summation of perturbation series was performed in[35] in order to recover the exact scaling exponents for conductance for one impurity. The results were used for the RG analysis of Y-junction [36–38] and generalized to arbitrary number of wires [39]. The contact of two helical TLL and tunneling from unpolarized spinful wire into the helical edge state was considered in [40]. The agreement between bosonization and fermionic approaches has been obtained when the comparison was available.

In the present paper we focus on the spin-polarized tunneling into the helical edge state. This problem was previously studied within bosonization approach[15], with the setup consisting of a point contact between fully spin-polarized tip and the helical edge state (see Fig.1). Generally, spin polarization in the tip differs from the

spin direction of the edge state fermions by some angle, ξ. In the absence of interaction this angle defines the left-right current asymmetry of the injected current. The charge fractionalization was demonstrated for the injection of electrons even with polarization parallel to the edge states in case on infinite helical TLL without Fermi liquid leads. Generalization of this result to time-dependent injected pulses was done in[16]. The effect of metallic leads for the visibility of fractionalization phenomena in transport measurement in helical TLL was analyzed in [18]. It was argued there that the fractionalization cannot be observed for dc currents, while information about helical TLL physics can be extracted from studying the transient dynamics.

In our approach below we use the fermionic formalism of scattering states, which implies the existence of Fermi liquid leads. It results in the absence of charge fractionalization in dc limit for the parallel polarization of the tip. For non-parallel polarization we show that the left-right asymmetry of the dc current, injected to helical TLL, is not defined entirely by the polarization angle but is renormalized along with the total tunneling conductance, with the resulting coupled RG equations. The asymmetry renormalization appears in first order of interaction strength and first order of tunneling conductance, and we discuss it to some detail. Simultaneous renormalization of two quantities is tied to the existence of saddle point RG fixed point (FP) in the phase portrait of the system.[41] In the absence of backscattering in the helical TLL, this non-universal FP separates two truly stable FPs. This in turn may lead to qualitatively different renormalization of asymmetry and total tunneling rate for different interaction strength.

The plan of the paper is as follows. We define the needed ingredients of our formalism in Sec. II with the discussion of the Hamiltonian, conductance matrix and the full RG equation set. The analysis of renormalization of spin-polarized tunneling is performed in Sec. III with increasing level of sophistication. We start with the first order calculation and proceed to full scaling curve analysis and to RG phase portrait of the system. The concluding remarks are presented in Sec. IV. The connection between the general form of S matrix and its particular simpler forms is discussed in Appendix .

II. THEORETICAL FORMALISM

A. The model

We consider Y-junction of the quantum wires shown in Fig. 1. Two quantum wires labeled by $j = 1, 2$ correspond to the TI helical edge state and the wire with $j = 3$ is the tunneling tip with fully polarized electrons. The polarization vector of electrons in the tip is different from the quantization axis in the TI edge state. We denote this difference by the angle ξ, so that $\xi = 0(\pi)$ describes the tip polarization parallel (antiparallel) to the right-moving fermions in the edge state.

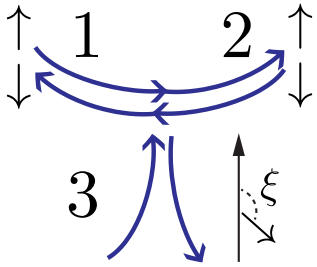

FIG. 1: Schematically shown scanning tunneling microscopy of the helical edge state of topological insulator by the spin-polarized tip. ξ is an angle between electron spin in the tip and spin quantization axis of the helical state.

The helical state of the main wire is described by the TLL model with the interaction between electrons of short-range forward-scattering type. We assume that the electronic interaction in the main wire is absent in the vicinity of the junction. This model simplification serves as a regularization of the theory at short distances and is encoded in length ℓ of the order of the Fermi wave length. All three quantum wires of length L are adiabatically connected to the reservoirs or leads such that additional scattering is absent. Scattering electron states flowing in and out the junction are connected by the S matrix.

TLL model Hamiltonian with linearized spectrum near the Fermi energy and in the scattering states formalism reads

$$\begin{aligned} \mathcal{H} &= \int_0^\infty dx[H^0 + H^{int}\Theta(\ell < x < L)]\,, \\ H^0 &= v_F\Psi^\dagger_{in} i\nabla\Psi_{in} - v_F\Psi^\dagger_{out} i\nabla\Psi_{out}\,, \\ H^{int} &= 2\pi v_F \sum_{j=1}^{3} g_j \widehat{\rho}_j \widehat{\widetilde{\rho}}_j\,. \end{aligned} \tag{1}$$

Here we introduce window function $\Theta(\ell < x < L)$ such that $\Theta(x) = 1$, if $\ell < x < L$ and zero otherwise. Density operators are defined by $\widehat{\rho}_{j,in} = \Psi^+\rho_j\Psi = \widehat{\rho}_j$, and $\widehat{\rho}_{j,out} = \Psi^+\widetilde{\rho}_j\Psi = \widehat{\widetilde{\rho}}_j$, where $\widetilde{\rho}_j = S^+ \cdot \rho_j \cdot S$ and the density matrices are given by $(\rho_j)_{\alpha\beta} = \delta_{\alpha\beta}\delta_{\alpha j}$ and $(\widetilde{\rho}_j)_{\alpha\beta} = S^+_{\alpha j}S_{j\beta}$. Electron interaction constant in the edge state is defined by $g_1 = g_2 = g$ and $g_3 = 0$ in the tip ; we set $v_F = 1$ below.

Ingoing and outgoing electronic waves $\psi_{j,\mathrm{in}}, \psi_{j,\mathrm{out}}$ are connected at the junction by the S matrix $\Psi_{out}(x) = S \cdot \Psi_{in}(x)$ at $x \to 0$, where $\Psi_{in(out)} = (\psi_{1,in(out)}, \psi_{2,in(out)}, \psi_{3,in(out)})$. The S matrix characterizes the scattering in the junction and belongs to the unitary group $U(3)$. Our setup implies the chiral property, $|S_{13}| = |S_{32}|$, $|S_{23}| = |S_{31}|$. Due to the time-reversal invariance of TI, the backscattering in the edge state without the tip is forbidden. The same is true in case when the polarization of the tip is parallel to the spin direction of right or left mover, $\xi = 0, \pi$.

In general, the chiral S-matrix is characterized by three parameters[38]. The absence of backscattering reduces the appropriate S matrix to the following two-parametric form

$$
\begin{aligned}
S &= \begin{pmatrix} r_1 & t_{12} & t_{13} \\ t_{21} & r_1 & t_{23} \\ t_{31} & t_{32} & r_2 \end{pmatrix} \\
r_1 &= \sin^2\frac{\theta}{2}\sin\xi, \quad r_2 = \cos\theta, \\
t_{12} &= -\cos\theta\cos^2\frac{\xi}{2} - \sin^2\frac{\xi}{2}, \quad t_{21} = t_{12}|_{\xi\to\pi-\xi}, \\
t_{13} &= t_{32} = \cos\frac{\xi}{2}\sin\theta, \quad t_{23} = t_{31} = \sin\frac{\xi}{2}\sin\theta.
\end{aligned} \tag{2}
$$

One parameter, θ, is responsible for the tunneling amplitude and $\theta = 0$ corresponds to the fully detached tip, in this case there is a perfect transmission through the edge state. Second parameter ξ is the above angle between electron spin in the tip and spin quantization axis of the helical state, see Appendix.

B. Reduced conductances

In linear response regime the conductances are defined by $I_i = C_{ik}V_k$ where I_j and V_j are the current flowing towards in the junction and the electric potential in jth lead, respectively. In the dc limit one easily obtains from Kubo formula $C_{ij} = \delta_{ij} - Y_{ij}$, with $Y_{ij} = |S_{ij}|^2$. The total current conservation and the absence of current for equal voltages lead to conditions $\sum_i C_{ij} = \sum_j C_{ij} = 0$, which also stem from the unitarity of S-matrix. It means that we can introduce new current and voltage combinations to show the condition explicitly.[42]

We choose new combinations according to relations $I_i^{\rm new} = \sum_k R_{ki} I_k$, $V_i^{\rm new} = \sum_k R_{ki} V_k$, where the matrix

$$
\mathbf{R} = \begin{pmatrix} \frac{1}{\sqrt{2}} & \frac{1}{\sqrt{6}} & \frac{1}{\sqrt{3}} \\ -\frac{1}{\sqrt{2}} & \frac{1}{\sqrt{6}} & \frac{1}{\sqrt{3}} \\ 0 & -\sqrt{\frac{2}{3}} & \frac{1}{\sqrt{3}} \end{pmatrix} \tag{3}
$$

has properties $\mathbf{R}^{-1} = \mathbf{R}^T$, $\det \mathbf{R} = 1$.

The corresponding matrix of conductances $\mathbf{C}^R = \mathbf{R}^T\,\mathbf{C}\,\mathbf{R}$ for the above form of S, Eq. (2), becomes

$$
\mathbf{C}^R = \begin{pmatrix} 1-a & -c & 0 \\ c & 1-b & 0 \\ 0 & 0 & 0 \end{pmatrix}. \tag{4}
$$

with

$$
\begin{aligned}
a &= \tfrac{1}{2}(1+\cos^2\theta)\cos^2\xi - \cos\theta\sin^2\xi, \\
b &= \tfrac{1}{4}(1+3\cos 2\theta), \\
c &= \tfrac{\sqrt{3}}{2}\cos\xi\sin^2\theta.
\end{aligned} \tag{5}
$$

It is convenient to analyze the quantity $\mathbf{Y}^R = 1 - \mathbf{C}^R$ below. Clearly, only two components of $\mathbf{Y}^R$ are independent. The chiral component of conductance, c, depends on the asymmetry parameter, $\cos\xi$, which includes the polarization angle, ξ.

We can also introduce more "physical" combinations of currents, $\mathbf{I}^{\rm phys} = (I_a, I_b)$, and voltages, $\mathbf{V}^{\rm phys} = (V_a, V_b)$, as

$$
\begin{aligned}
I_a &= \tfrac{1}{2}(I_1 - I_2)\,, & I_b &= \tfrac{1}{3}(I_1 + I_2 - 2I_3)\,, \\
V_a &= V_1 - V_2\,, & V_b &= \tfrac{1}{2}(V_1 + V_2 - 2V_3)\,.
\end{aligned} \tag{6}
$$

In terms of these, the matrix of conductances $\mathbf{I}^{\rm phys} = \mathbf{G}\mathbf{V}^{\rm phys}$ is given by

$$
\mathbf{G} = \begin{pmatrix} G_a & G_{ab} \\ G_{ba} & G_b \end{pmatrix} = \begin{pmatrix} \frac{1}{2}(1-a) & -\frac{c}{\sqrt{3}} \\ \frac{c}{\sqrt{3}} & \frac{2}{3}(1-b) \end{pmatrix}. \tag{7}
$$

with the property, $0 \le G_{a,b} \le 1$, see[42].

C. Renormalization group equations

The dc transport through the chiral Y-junction was studied in fermionic formalism in[37,38]. We sketch here the derivation of the corresponding formulas. The principal first order interaction correction to the conductances reads[37]

$$
C_{jk} = C_{jk}\big|_{\mathbf{g}=0} + \tfrac{1}{2}\sum_{l,m} {\rm Tr}\left[\widehat{W}_{jk}\widehat{W}_{lm}\right] g_{ml}\Lambda\,, \tag{8}
$$

where we defined $C_{jk}|_{\mathbf{g}=0} = \delta_{jk} - Y_{jk}$, a matrix $g_{ml} = g_l\delta_{ml}$ with interaction constants g_l in the Hamiltonian (1), nine 3×3 matrices $\widehat{W}_{jk} = [\rho_j, \widetilde{\rho}_k]$ and the trace operation Tr is defined with respect to the 3×3 matrix space of $\widehat{W}$'s. The scale-dependent term $\Lambda = \ln(\min[L,\xi]/\ell)$ with the temperature correlation length $\xi = v_F/T$.

The above correction is the leading contribution, $\sim g\Lambda$, to conductance. It was shown[42] that the higher-order corrections obey the scaling hypothesis for the conductance and are generated by a set of the differential RG equations. In its simplest form, these equations are obtained by differentiating Eq. (8) over Λ (and then putting $\Lambda = 0$) which gives

$$
\frac{d}{d\Lambda}Y^R_{jk} = -\frac{1}{2}\sum_{l,m} {\rm Tr}\left[\widehat{W}^R_{jk}\widehat{W}^R_{lm}\right] g^R_{ml}\,, \tag{9}
$$

where all quantities with superscript R are defined as $\mathbf{A}^R = \mathbf{R}^T\,\mathbf{A}\,\mathbf{R}$.

The main source of linear-in-Λ subleading corrections corresponds to a ladder series of diagrams, which can be summed analytically[42]. These corrections are independent of the scheme of regularization in RG procedure and lead to the scaling exponents for conductances, coinciding with those obtained by bosonization method.

The result of the ladder summation[38,39] is the RG equation similar to above Eq. (9) with the replacement

$$
\mathbf{g} \to \bar{\mathbf{g}} = 2(\mathbf{Q} - \mathbf{Y})^{-1}\,. \tag{10}
$$

The matrix $\mathbf{Q}$ depends on the Luttinger parameters K_j of individual wires and has the form

$$\begin{aligned} Q_{jk} &= q_j\delta_{jk}\,, \quad q_j = (1+K_j)/(1-K_j)\,, \\ K_j &= [(1-g_j)/(1+g_j)]^{1/2}. \end{aligned} \tag{11}$$

In our case we have $g_1 = g_2 = g$ and $g_3 = 0$. The latter equality corresponds to $q_3 \to \infty$, which limit is easily taken in (10).

Now we are in a position to obtain RG equations of the conductances. However, the equivalent RG equations in terms of parametrization (2) have simpler form, and we choose it below. After some algebra we obtain from (5), (9), (10) the following set of equations

$$\begin{aligned} \frac{d\theta}{d\Lambda} &= -\frac{1}{8}(1-K)\sin\theta\frac{F_1(\theta)+F_2(\theta)\cos 2\xi}{F_3(\theta)D(\theta,\xi)}, \\ \frac{d\xi}{d\Lambda} &= \frac{1}{4}(1-K)\frac{(1-\cos\theta)\sin 2\xi}{D(\theta,\xi)}, \\ F_1 &= 2(1-K) - (3-K)\sin^2\tfrac{\theta}{2} \\ &\quad - 3(1-K)\sin^2\theta, \\ F_2 &= \sin^2\tfrac{\theta}{2}(2-3(1-K)\sin^2\tfrac{\theta}{2}), \\ F_3 &= 1-(1-K)\sin^2\tfrac{\theta}{2}, \\ D(\theta,\xi) &= K+(1-K)\sin^2\tfrac{\theta}{2}\left(1-\sin^2\tfrac{\theta}{2}\sin^2\xi\right). \end{aligned} \tag{12}$$

These equations are analyzed in the next section. Notice that the asymmetry parameter $p = \cos\xi$ is now determined not only by the initial polarization angle, but also by the interaction strength and tunneling amplitude.

III. SPIN-POLARIZED TUNNELING

A. Lowest order calculation

Let us first consider the limit of weak tunneling into the helical edge state. It means that both tunneling from the tip and the backscattering in the edge state due to this tunneling are approximately zero. In terms of the S matrix (2) we write $|r_2|^2 \simeq 1$ and $|r_1|^2 \simeq 0$. First condition gives $\theta \simeq 0$ or $\theta \simeq \pi$, and the second condition states that if $\theta \simeq \pi$ then $\xi \simeq 0$ or $\xi \simeq \pi$. These three seemingly unconnected regions form a neighborhood of the fixed point (FP) A, as is discussed below.

Confining ourselves to the linear-in- θ terms, we get from Eqs. (12):

$$\frac{d\theta}{d\Lambda} = -\frac{(1-K)^2}{4K}\theta\,, \qquad \frac{d\xi}{d\Lambda} = 0\,. \tag{13}$$

Hence, the parameter θ, which is related to the barrier transparency, is renormalized to zero with the scaling law $\theta = \theta_0\exp(-\nu\Lambda/2)$, and the tunneling exponent $\nu = (1-K)^2/2K$. The asymmetry ratio $t_\downarrow/t_\uparrow = \tan\xi/2$ is not renormalized.

This result is in exact agreement with the earlier work[15], where the renormalization of the tunnel amplitudes $t_\uparrow$ and $t_\downarrow$ was studied in the bosonization approach. Equation (9) of the above paper obtains the currents flowing to the right I_R and to the left I_L ends of the edge state. One has

$$I_\mathrm{L} + I_\mathrm{R} = I_0\,, \qquad I_\mathrm{L} - I_\mathrm{R} = -KI_0\cos\xi\,. \tag{14}$$

In our notation (6) the current I_0 equals to I_b, and the difference of the currents $I_\mathrm{L} - I_\mathrm{R}$ is $2I_a$. For zero bias in the edge state, $V_a = 0$, we have $I_b = G_bV_b$, $I_a = G_{ab}V_b$ and obtain from Eqs. (5), (7) :

$$2I_a = -I_b\cos\xi \tag{15}$$

This equation coincides with (14) apart from the factor K, which is absent in dc limit in our setup with the Fermi leads. The absence of this factor in similar setup was also obtained in the work [18] in bosonization approach.

Now we consider the next terms in the expansion of RG equations in θ. Quadratic-in θ term appears only in RG equation for asymmetry angle:

$$\frac{d\xi}{d\Lambda} = \frac{1-K}{8K}\theta^2\sin 2\xi. \tag{16}$$

Solution of the equation shows that the asymmetry angle is renormalized according to the law

$$\tan\xi = \tan\xi_0 e^{-(\theta^2-\theta_0^2)/2(1-K)}. \tag{17}$$

Since θ is renormalized to zero (see eq. (13)), we find the whole renormalization of ξ insignificant for small bare tunneling amplitude θ_0. At the same time the renormalization of ξ in (16) is first order interaction effect for small interaction $\frac{1-K}{K} \approx g \ll 1$, whereas the tunneling exponent for θ in Eq. (13) is given by the second order of interaction, $\frac{(1-K)^2}{K} \approx g^2$.

We see that if we discard the small-in-θ terms in RG equation for ξ, then we do not obtain renormalization of asymmetry at all. However the smallness-in-θ may be compensated by the less power of interaction in the RG flow of ξ. As a result for small interaction and tunneling amplitude the renormalization of θ and ξ may be of the same order as demonstrated in Fig. 2.

We also note here that Eq. (17) can be rewritten in terms of the asymmetry $p = \cos\xi$ as

$$\frac{dp}{d\Lambda} = -\frac{1-K}{4K}\theta^2 p(1-p^2). \tag{18}$$

This equation possesses three fixed points (FPs) $p = 0, \pm 1$, and if θ^2 were non-vanishing at $\Lambda \to \infty$, then we would obtain only $p = 0$ as a stable FP for repulsive interaction, $K < 1$. In the leading order of interaction, we can combine first equation in (13) and (18) to represent the RG trajectory in the form

$$\theta^2 - g\log\frac{p^2}{1-p^2} = \text{const}. \tag{19}$$

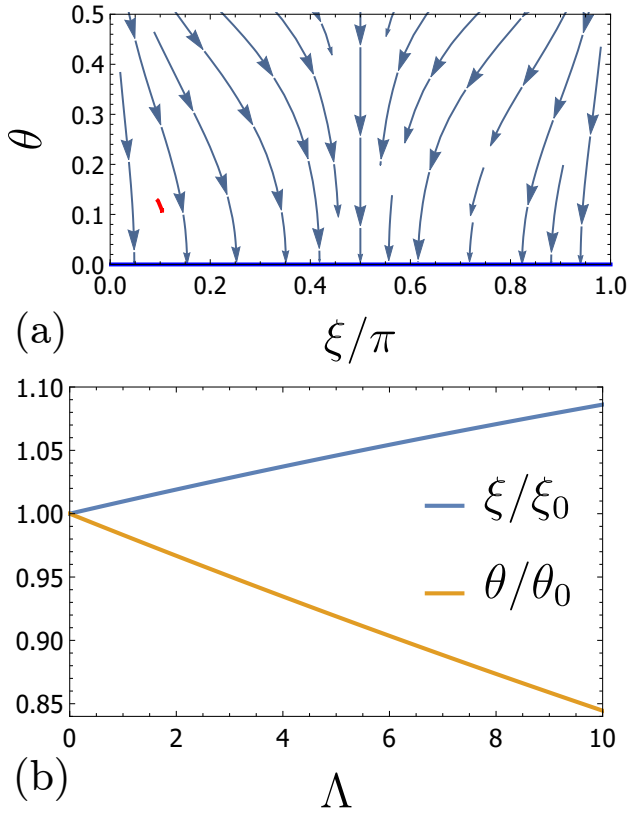

FIG. 2: The panel (a) shows RG flows in the plane $(\xi,\ \theta)$ for $g = 0.26$ ($K = 0.77$). Relative renormalization of ξ and θ for this flow and $\xi_0 = 0.3$, $\theta_0 = 0.4$ is shown in panel (b).

B. M point

The terms of the order θ^3 appear only in the equation for θ :

$$\frac{d\theta}{d\Lambda} = -\frac{(1-K)^2}{4K}\theta + \frac{(1-K)(\kappa-\cos 2\xi)}{16K}\theta^3, \qquad (20)$$

where $\kappa \equiv (1-K)(2/3+K)+1/K$. For small interaction $\kappa \approx 1$ and the equation (20) becomes

$$\frac{d\theta}{d\Lambda} = -\frac{g^2}{4}\theta + \frac{g(1-\cos 2\xi)}{16}\theta^3. \qquad (21)$$

First, one can see here that the θ^3 -term is unimportant in parallel polarization case, $\xi = 0, \pi$; the right-hand side of Eq. (16) is zero. Thus the lines $\xi = 0, \pi$ are RG fixed lines.

Otherwise the combination of (20) with (16) reveals the existence of non-universal fixed point M at $\xi_M = \pi/2$, $\theta_M \approx \sqrt{2g}$. Similar to above Eq. (16), the next order term in θ expansion contains smaller power of interaction strength. This situation was discussed for non-chiral symmetric Y-junction in[41].

Solving RG equations for asymmetry p and θ gives for the RG trajectory

$$\theta^2 p - g\log\frac{1+p}{1-p} = \text{const}\,. \qquad (22)$$

TABLE I: The position of universal fixed points.

θ	0	π	π	π	$\pi/2$	$\pi/2$
ξ	arb.	0	π	$\pi/2$	0	π
G_a	1	1	1	0	3/4	3/4
G_b	0	0	0	0	1	1
G_{ab}	0	0	0	0	1/2	$-1/2$
FP	A	A	A	N	χ^-	χ^+

Despite the apparently different form of Eqs. (22) and (19), these equations yield numerically close curves for small $\theta < \theta_M$. Indeed the existence of the next term in equation (20) does not seriously affect RG flows in this limit.

Already at the level of approximate Eqs. (20), (16) one can expect that for $\theta \approx \theta_M$ the RG flow for the asymmetry $\cos\xi$ may exceed the RG flow of barrier transparency θ. We discuss this point in more detail in the next subsection.

C. Full scaling dependence

Now we go beyond the weak tunneling approximation and discuss the general RG Eqs. (12) for $K < 1$. In this rather complicated case we have five universal FPs in the (θ,ξ)-plane, one interaction dependent (i.e. non-universal) fixed point M ($\xi_M = \pi/2, \theta_M = \arccos\frac{1}{3}\left(\sqrt{q_1^2+6q1-3}-q_1\right)$ and the lines of fixed points ($\xi \in (0,\pi)$ and $\theta = 0$), see Fig. 3 and Tab. I. The points $(\xi = 0, \theta = \pi)$, $(\xi = \pi, \theta = \pi)$ and the fixed line $\theta = 0$ correspond to one point A in terms of conductances.

For repulsive electron interaction the fixed line $\theta = 0$ (the point A) is stable and corresponds to effective detachment of the tip from the edge state. It exists simultaneously with the stable point N which corresponds to full breaking of the junction. The line in (ξ,θ) plane which separates these two basins of attraction connects the unstable points $\chi^\pm$ with the saddle point M (see Fig. 3). The chiral FPs $\chi^\pm$ were discussed in detail in[28,38] they become stable for attractive interaction.

One may ask why the same point A described as $\theta = 0$ is stable and at the same time unstable when parametrized by $\theta = 0$, $\xi = 0(\pi)$. This situation is clarified by considering the surface of conductances in Fig. 5. It is seen that domains of different character (stable and unstable) near the point A are separated by three ridges. Two of them are the lines $\xi = 0$, $\theta \in (0,\pi)$ and $\xi = \pi$, $\theta \in (0,\pi)$ depicted by the red lines on the conductances surface, the third ridge connects A and N points. The domain 1 corresponds to $\theta \approx 0$ and the domain 2 (3) corresponds to $\theta \approx \pi$ but $\xi \approx 0(\pi)$. All these ridges are RG fixed lines, and any RG flow starting on these lines continues along them. It also means that any RG flow

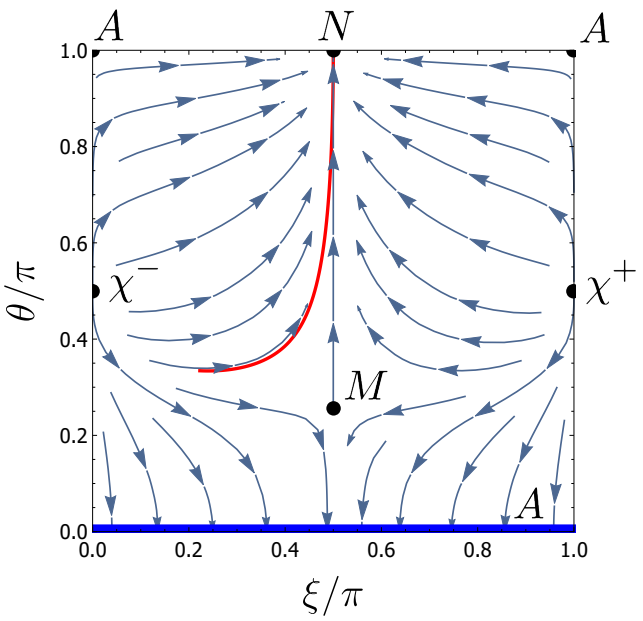

FIG. 3: RG flows (blue arrows) demonstrate the simultaneous existence of the stable fixed line (blue line) at point A and stable point N, depending on the initial conditions (ξ, θ) for electron interaction $g = 0.72$ ($K = 0.4$). Red line corresponds to the RG flow plotted in terms of conductances in Fig. 4b.

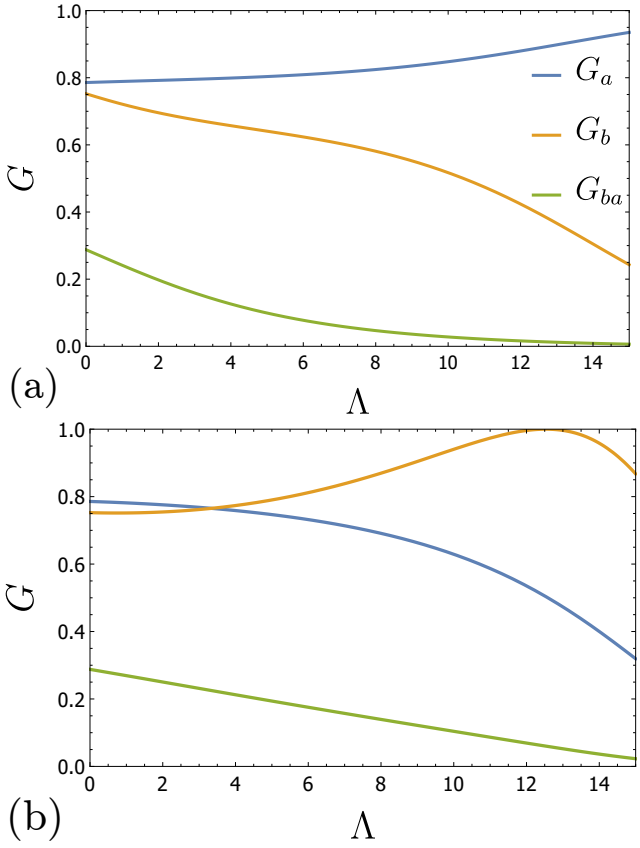

FIG. 4: Full scaling curves for conductances are shown in panel (a) for electron interaction $g = 0.47$ ($K = 0.6$). The RG flow corresponds to going to the point A, i.e. effective detachment of the tip. The panel (b) shows the RG flows for stronger electron interaction $g = 0.72$ ($K = 0.4$). The conductances are renormalized to the point N, i.e. effective full breaking of the junction. Bare initial conductances on both panels are the same and the qualitative change in the RG flows is caused by the change in the interaction strength.

cannot pass across these ridges.

The whole plane (θ, ξ) is divided into two regions in Fig. 3, depending on the interaction strength. One region corresponds to a basin of attraction to the point N, another – to the point A. The situation is similar to purely tunneling case (PTC) for symmetric non-chiral Y-junction[41]. It was shown there that for PTC the points A or N are stable and separated by the unstable M point. Any deviation from PTC, which means the backscattering in the main wire, leads to an additional RG flow driving the junction to truly stable N point while A becomes of saddle point type. In our present model we have the chiral PTC junction, and any additional modification of S-matrix is forbidden due to topological character of edge state and the absence of backscattering in the main wire.

Notice that for vanishing interaction, g, the FPs A and M merge, and the basin of attraction for A point vanish. More precisely, A point becomes saddle-point type in this limit and is stable only for parallel polarization of the tip, $\xi = 0, \pi$. All RG trajectories in this limit obey the equation

$$\cos\xi \tan^2(\theta/2) = \text{const}. \tag{23}$$

Two examples of full scaling curves for conductances calculated for sizable interaction strength are shown in Fig. 4. The values of bare conductances are the same, but the panel (a) demonstrates RG flows going to the point A, whereas the panel (b) shows the system driven to the point N. This difference stems from the fact that changing interaction strength shifts the separating curve between the basins of attraction of corresponding FPs.

For completeness we provide here the scaling exponents at the FPs A and N. The scaling exponent for the point A depends on the direction of approach to this FP as explained above. In the domain 1 in Fig. 5 i.e. at $\theta \simeq 0$ we have only one scaling exponent for θ, equal to $(1-K)^2/4K$. In the domains 2 and 3 in Fig. 5, i.e. at the points $\theta = \pi$, $\xi = 0(\pi)$ we have additional scaling exponent, the RG flows away from A point along ξ with a weak impurity exponent $(1-K)$. Near the stable N point the exponents along θ and ξ are $\frac{1}{2}(K^{-1}-1)$ and $(K^{-1}-1)$.

IV. CONCLUSIONS

We analyzed the simultaneous renormalization of asymmetry and total tunneling conductance from fully

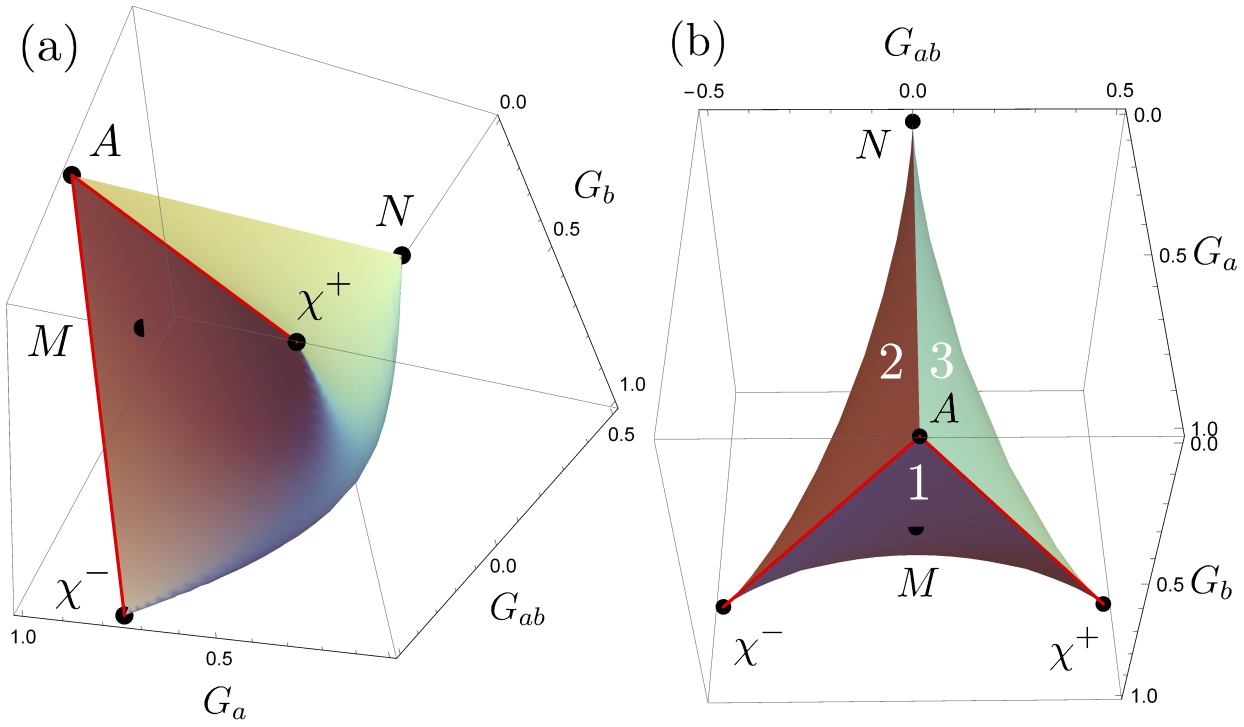

FIG. 5: 2D fixed surface of physical conductances (7) in 3D conductances space is shown. Fixed points are depicted by black dots. Fixed lines corresponding to $\xi = 0$, $\theta \in (0, \pi)$ and $\xi = \pi$, $\theta \in (0, \pi)$ are shown in red. The panel (b) shows that three domains near the point A are separated by ridges, which cannot be crossed by any RG flow. This explains why the point A is stable for repulsive electron interaction in the domain 1 ($\theta \approx 0$), and at the same time unstable in domains 2 and 3 ($\theta \approx \pi$, $\xi \approx 0(\pi)$).

polarized tip into the helical edge state. In particular we showed that the RG flow for these two quantities is sensitive to the appearance of non-universal FP with asymmetry $\cos \xi_M = 0$ and tunneling conductance $G_b \simeq \theta_M^2 \simeq 2g$ for small interaction, g.

Our method assumes the existence of Fermi leads, which are needed for consistent definition of the S-matrix describing the Y-junction in terms of asymptotically free states. Experimentally it can be realized by the extended leads over the helical edge state. The helical edge state, on the other hand, is a topological object which cannot have disconnected ends. The dc current injected from the tunneling tip into the edge state may exit at another drain Y-junction. This means the ring geometry with potentially important interference effects. The above picture of the renormalization of the single Y-junction should be valid when the temperature correlation length $\xi = v_F/T$ is smaller than the circumference of the edge state multiplied by $|r_1|^2$. The importance of interference effects is then reduced[43] but the corresponding analysis is beyond the scope of this study.

Acknowledgments

We are grateful to P. Wölfle, D.B. Gutman and V.Yu. Kachorovskii for useful discussions. This work was partly supported by RFBR grant No 15-52-06009. The work of D.A. was supported by Russian Science Foundation Grant (Project No. 14-22-00281).

Appendix: Rotation of polarization axes

Our setup depicted in Fig. 1 is characterized by the angle ξ between spin quantization axis in helical edge states and polarization direction in the tip. One can show that two-parametric S matrix (2) can be obtained from one-parametric one by rotation of the edge states basis. The Kramers spinor of scattered states is given by rearrangement of out- states, $\psi_{1,out} \leftrightarrow \psi_{2,out}$, by the matrix

$$F = \begin{pmatrix} 0 & 1 & 0 \\ 1 & 0 & 0 \\ 0 & 0 & 1 \end{pmatrix}. \tag{A.1}$$

The rotation of spin quantization axes is described by

$$U = \begin{pmatrix} e^{\frac{1}{2}i(\alpha+\gamma)} \cos\frac{\beta}{2} & e^{-\frac{1}{2}i(\alpha-\gamma)} \sin\frac{\beta}{2} & 0 \\ -e^{\frac{1}{2}i(\alpha-\gamma)} \sin\frac{\beta}{2} & e^{-\frac{1}{2}i(\alpha+\gamma)} \cos\frac{\beta}{2} & 0 \\ 0 & 0 & 1 \end{pmatrix}, \tag{A.2}$$

where the upper left 2×2 matrix is $e^{i\gamma\sigma_3/2} e^{i\beta\sigma_2/2} e^{i\alpha\sigma_3/2}$ with α, β, γ are Euler angles and $\sigma_{2,3}$ Pauli matrices.

For injected spin polarization parallel to the helical edge state, $\xi = 0$, the form of S matrix is simplified :

$$S_\uparrow = \begin{pmatrix} 0 & -\cos\theta & \sin\theta \\ -1 & 0 & 0 \\ 0 & \sin\theta & \cos\theta \end{pmatrix}. \quad \text{(A.3)}$$

If $\xi \neq 0(\pi)$ then we have to rotate the quantization basis of the helical edge states:

$$S = US_\uparrow FU^\dagger F. \quad \text{(A.4)}$$

The dependence of rotated S matrix on angles α and γ is removed by additional rephasing. The matrix (A.4) coincides with (2) after the substitution $\beta \to -\xi$.

In our paper [40] the tunneling from the unpolarized tip into the helical edge states was discussed. This X junction was modeled by 4×4 S matrix since there are two spin channels in unpolarized case. It was shown that a certain ratio of the conductances is not renormalized, see equation (26) in[40]. Applying the above arguments to the situation with X-junction, we confirm that the discussed ratio corresponds to the angle between the quantization axes for helical edge states and the tip (the quantity -2γ in[40] is the above Euler angle β). This observation clarifies the scale invariance of the ratio, as the choice for the spin quantization basis can be made arbitrarily without changing physical consequences.

The case of the corner X-junction between two helical edge states [40] can also be discussed in terms of quantization axes rotation. Three stable FPs were obtained for repulsive interaction. One of them corresponds to the detachment of helical edge states independent of directions of the spin quantization axes. Two other FPs correspond to cases of parallel ($\beta = 0$) or antiparallel ($\beta = \pi$) orientation of the quantization axes in individual edges. The choice between these FPs is defined by the value of relative orientation without interaction, $\beta < \pi/2$ or $\beta > \pi/2$, respectively.

[1] M. Z. Hasan and C. L. Kane, Rev. Mod. Phys. **82**, 3045 (2010).
[2] X.-L. Qi and S.-C. Zhang, Rev. Mod. Phys. **83**, 1057 (2011).
[3] T. Giamarchi, *Quantum Physics in One Dimension* (Clarendon Press, Oxford, 2003).
[4] B. Braunecker, C. Bena, and P. Simon, Phys. Rev. B **85**, 035136 (2012).
[5] M. Kharitonov, Phys. Rev. B **86**, 165121 (2012).
[6] A. Soori, S. Das, and S. Rao, Phys. Rev. B **86**, 125312 (2012).
[7] G. Dolcetto, F. Cavaliere, D. Ferraro, and M. Sassetti, Phys. Rev. B **87**, 085425 (2013).
[8] A. Calzona, M. Carrega, G. Dolcetto, and M. Sassetti, Phys. Rev. B **92**, 195414 (2015).
[9] A. Calzona, M. Acciai, M. Carrega, F. Cavaliere, and M. Sassetti, Phys. Rev. B **94**, 035404 (2016).
[10] S.-P. Chao, S. A. Silotri, and C.-H. Chung, Phys. Rev. B **88**, 085109 (2013).
[11] G. Dolcetto, N. T. Ziani, M. Biggio, F. Cavaliere, and M. Sassetti, physica status solidi (RRL) - Rapid Research Letters **7**, 1059 (2013).
[12] H. Steinberg, G. Barak, A. Yacoby, L. N. Pfeiffer, K. W. West, B. I. Halperin, and K. L. Hur, Nat Phys **4**, 116 (2007).
[13] K. L. Hur, B. I. Halperin, and A. Yacoby, Annals of Physics **323**, 3037 (2008).
[14] S. Pugnetti, F. Dolcini, D. Bercioux, and H. Grabert, Phys. Rev. B **79**, 035121 (2009).
[15] S. Das and S. Rao, Phys. Rev. Lett. **106**, 236403 (2011).
[16] I. Garate and K. Le Hur, Phys. Rev. B **85**, 195465 (2012).
[17] U. Khanna, S. Pradhan, and S. Rao, Phys. Rev. B **87**, 245411 (2013).
[18] A. Calzona, M. Carrega, G. Dolcetto, and M. Sassetti, Physica E: Low-dimensional Systems and Nanostructures **74**, 630 (2015).
[19] R. A. Santos, D. B. Gutman, and S. T. Carr, Phys. Rev. B **93**, 235436 (2016).
[20] J.-V. Kim, F. Garcia-Sanchez, J. a. Sampaio, C. Moreau-Luchaire, V. Cros, and A. Fert, Phys. Rev. B **90**, 064410 (2014).
[21] T. Li, P. Wang, H. Fu, L. Du, K. A. Schreiber, X. Mu, X. Liu, G. Sullivan, G. A. Csáthy, X. Lin, et al., Phys. Rev. Lett. **115**, 136804 (2015).
[22] R. Wu, J.-Z. Ma, S.-M. Nie, L.-X. Zhao, X. Huang, J.-X. Yin, B.-B. Fu, P. Richard, G.-F. Chen, Z. Fang, et al., Phys. Rev. X **6**, 021017 (2016).
[23] T. Giamarchi and H. J. Schulz, Phys. Rev. B **37**, 325 (1988).
[24] A. Furusaki and N. Nagaosa, Phys. Rev. B **47**, 4631 (1993).
[25] C. L. Kane and M. P. A. Fisher, Phys. Rev. B **46**, 15233 (1992).
[26] K. A. Matveev, D. Yue, and L. I. Glazman, Phys. Rev. Lett. **71**, 3351 (1993).
[27] D. Yue, L. I. Glazman, and K. A. Matveev, Phys. Rev. B **49**, 1966 (1994).
[28] M. Oshikawa, C. Chamon, and I. Affleck, J. Stat. Mech. **2006**, P02008 (2006).
[29] C.-Y. Hou, A. Rahmani, A. E. Feiguin, and C. Chamon, Phys. Rev. B **86**, 075451 (2012).
[30] C.-Y. Hou, E.-A. Kim, and C. Chamon, Phys. Rev. Lett. **102**, 076602 (2009).
[31] J. C. Y. Teo and C. L. Kane, Phys. Rev. B **79**, 235321 (2009).
[32] A. Ström and H. Johannesson, Physical Review Letters **102**, 096806 (2009).
[33] S. Lal, S. Rao, and D. Sen, Phys. Rev. B **66**, 165327 (2002).
[34] S. Das, S. Rao, and D. Sen, Phys. Rev. B **70**, 085318 (2004).
[35] D. N. Aristov and P. Wölfle, Phys. Rev. B **80**, 045109 (2009).
[36] D. N. Aristov, Phys. Rev. B **83**, 115446 (2011).
[37] D. N. Aristov and P. Wölfle, Phys. Rev. B **86**, 035137 (2012).

[38] D. N. Aristov and P. Wölfle, Phys. Rev. B **88**, 075131 (2013).
[39] D. N. Aristov and P. Wölfle, Lith. J. Phys. **52**, 89 (2012).
[40] D. N. Aristov and R. A. Niyazov, Phys. Rev. B **94**, 035429 (2016).
[41] D. N. Aristov, A. P. Dmitriev, I. V. Gornyi, V. Y. Kachorovskii, D. G. Polyakov, and P. Wölfle, Phys. Rev. Lett. **105**, 266404 (2010).
[42] D. N. Aristov and P. Wölfle, Phys. Rev. B **84**, 155426 (2011).
[43] A. P. Dmitriev, I. V. Gornyi, V. Y. Kachorovskii, and D. G. Polyakov, Phys. Rev. Lett. **105**, 036402 (2010).